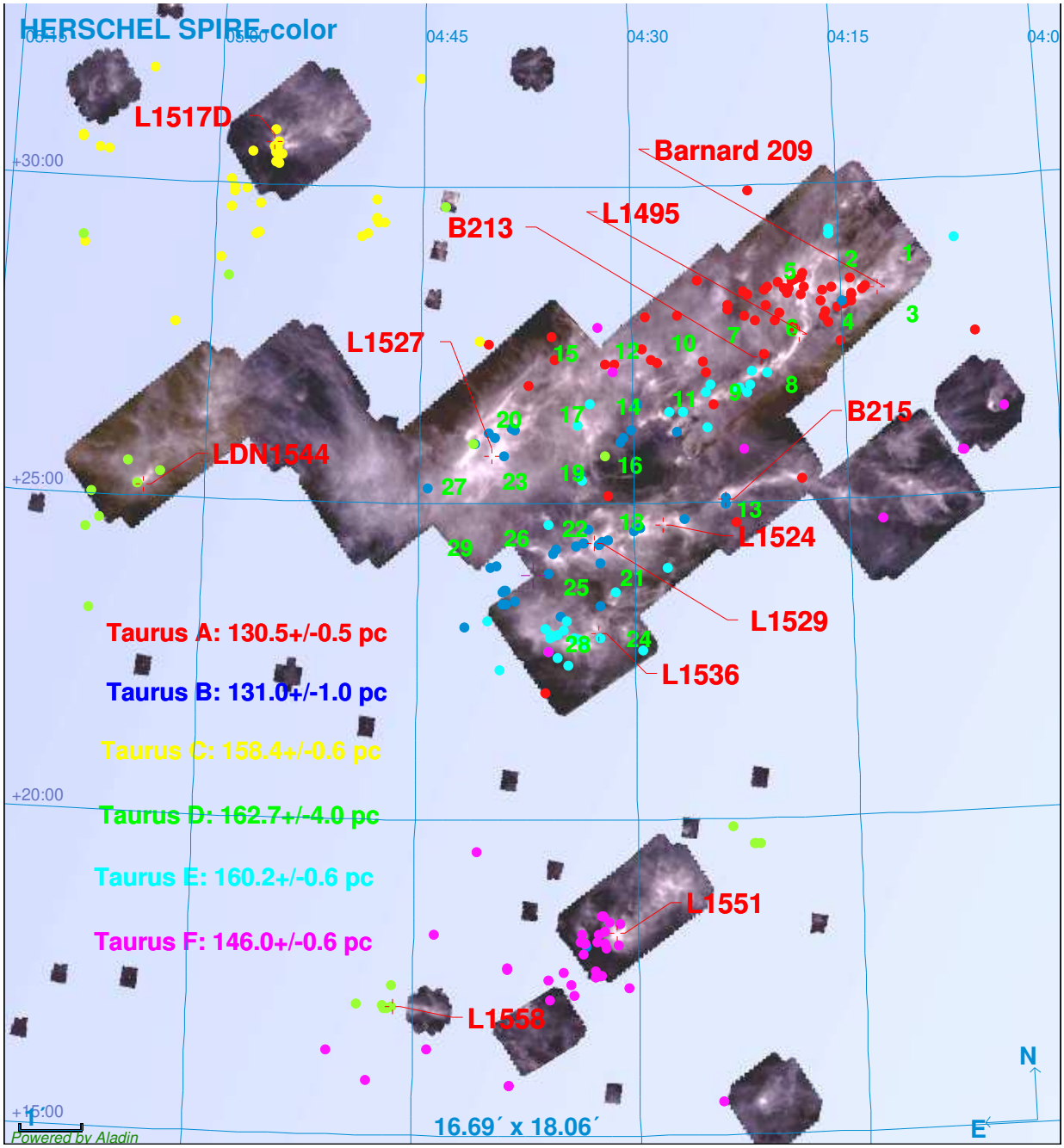

Fig. 6. *Herschel* RGB color composition using all public SPIRE observations from the Herschel Science Archive at 250 μm (blue), 350 μm (green), and 500 μm (red). The filled circles represent the most probable members of Taurus A (in red), Taurus B (in blue), Taurus C (in yellow), Taurus D (in green), Taurus E (in cyan) and Taurus F (in magenta). With *Taurus Main* we refer to the Taurus complex excluding the clouds L1517D, LDN 1551 and L1558. The green numbers which appear only on *Taurus Main* correspond to the distances in parsec computed in those positions by Zucker et al. (2019). In red we indicate the names of the clouds in the region. At 150 pc the size of 1° corresponds to 2.6 pc.

to bracket the dust screen between unreddened foreground stars and reddened background stars. The work of Zucker et al. (2019) allowed the authors to not only find a single distance for the surface of the Taurus molecular cloud of 141 ± 9 pc, but also to map the 3D surface of the region previously defined as *Taurus Main*. This discussion can be taken a step further by considering the 29 local distances computed by Zucker et al. (2019) over *Taurus Main* at the positions indicated with numbers 1–29 in the central part of Fig. 6. The values of the corresponding distances are given in Table 2. In the following, we take into account the measurement errors on both the stellar populations and the molecular cloud when comparing their relative positions. Most of the sources of Taurus A lie between the B209 and L1495 clouds: the stellar population, at 130 pc, is associated with the molecular cloud, which ranges between 132 and 136 pc. Taurus B extends over a filamentary structure, identified by a first filament corresponding to B215 and a second filament corresponding to L1524 and L1529. In this case, the stellar population is located in front of both filaments at a range of distances between 4 and 20 pc. A further six sources of Taurus B correspond instead to the L1527 cloud, and are associated with it, within the errors.

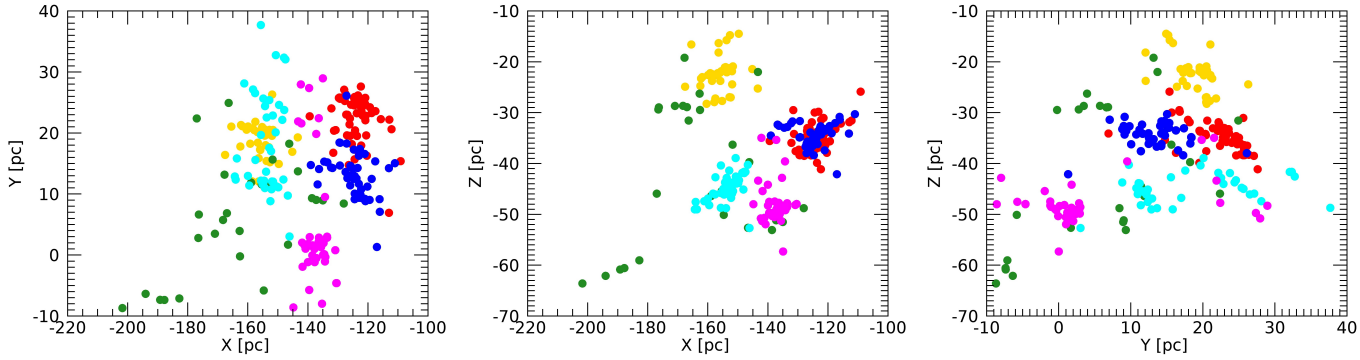

Fig. 7. Two-dimensional projections of the 3D spatial distribution of the multiple populations of Fig. A.1. The color code is as in Fig. 4.

Table 2. Local distances in *Taurus Main* computed by Zucker et al. (2019) with: the number appearing in Fig. 6 (Cols. 1 and 4), galactic positions (Cols. 2 and 5), and the distances (Cols. 3 and 6).

#	l [°] , b [°]	D [pc]	#	l [°] , b [°]	D [pc]
1	167.3, −16.3	133^{+3}_{-2}	16	173.0, −15.1	139^{+16}_{-14}
2	168.0, −15.7	116^{+17}_{-15}	17	173.0, −13.9	127^{+5}_{-4}
3	168.0, −17.0	132^{+6}_{-7}	18	173.7, −15.7	142^{+8}_{-4}
4	168.8, −16.3	136^{+8}_{-5}	19	173.7, −14.5	130^{+21}_{-4}
5	168.8, −15.1	136^{+13}_{-10}	20	173.7, −13.2	123^{+11}_{-6}
6	169.5, −15.7	132^{+2}_{-2}	21	174.4, −16.3	150^{+7}_{-6}
7	170.2, −15.1	142^{+3}_{-4}	22	174.4, −15.1	160^{+6}_{-8}
8	170.2, −16.3	162^{+10}_{-9}	23	174.4, −13.9	137^{+6}_{-4}
9	170.9, −15.7	152^{+4}_{-12}	24	175.1, −17.0	150^{+7}_{-6}
10	170.9, −14.5	114^{+10}_{-6}	25	175.1, −15.7	152^{+5}_{-6}
11	171.6, −15.1	128^{+3}_{-2}	26	175.1, −14.5	161^{+10}_{-9}
12	171.6, −13.9	154^{+4}_{-9}	27	175.1, −13.2	150^{+7}_{-6}
13	172.3, −17.0	151^{+4}_{-2}	28	175.8, −16.3	159^{+2}_{-1}
14	172.3, −14.5	147^{+4}_{-5}	29	175.8, −13.9	162^{+5}_{-4}
15	172.3, −13.2	126^{+6}_{-5}			

The part of Taurus E which in 2D appears to be associated with the L1495 and B213 filamentary structures is instead more distant by 2−20 pc at the center of the filamentary structure, and by 25−35 pc at its ends. The rest of Taurus E is on the surface of the L1536 cloud, at the same distance of about 160 pc.

Outside of *Taurus Main*, the distances of the individual clouds are not known. However, we find that Taurus C, at a distance of ∼160 pc, is spatially distributed on the L1517 cloud, while Taurus F is spatially distributed on L1551 and located at a distance of ∼146 pc, consistent with the mean distance of the Taurus molecular cloud. Assuming we have the same situation as in the case of L1527 and L1536, where the distances of the stellar populations correspond to the measured distances of the clouds, this might suggest that L1517 and L1551 lie at ∼160 pc and ∼146 pc, respectively, as do their associated stellar populations.

In this scenario, part of the different populations are still associated to the molecular cloud and the dynamical interactions between the stellar populations and the molecular cloud are still ongoing. It is important to note that the distances found for the molecular cloud represent only its upper layer closer to us. While the stellar population seems to be always associated with the clouds, this is not the case when filamentary structures are present.

A possible explanation is that the stellar population is moving away from the filamentary molecular cloud. Another possibility is that a physical mechanism actively removed the molecular cloud from the cluster. A further dedicated study is required to decipher which of the above mentioned scenarios has taken place in the Taurus complex, and to investigate the relation between star and clump formation and filaments in this region.

4.3. Kinematics of the Taurus Main populations

In the above discussion we conclude that only part of the stellar populations and the molecular cloud are still associated. In this section, we concentrate on the kinematics of the three populations associated with *Taurus Main*, namely Taurus A, B, and E. We use the available radial velocities collected from the literature by Galli et al. (2019). All three populations have radial velocity measurements for more than 20 stars; the corresponding histograms are shown in Fig. A.2. Although the accuracy of these measurements does not allow a proper investigation of possible subclusterings, we can in any case see that, while Taurus A and B share a similar peak of the distribution, the peak of Taurus E is shifted by ∼1 km s^{-1}.

We computed the galactic space velocity (U, V, W)[3] in the same reference system as the (*X,Y,Z*) positions computed in Sect. 4.2. These velocities have also been corrected for the solar motion[4] to the local standard of rest. We considered the mean 3D velocities between Taurus A, B, and E as a reference to compute the mean differential velocities of each population. The results are shown in Fig. 8 with the three projections of the 3D average motions on the planes (*X,Y*), (*X,Z*), and (*Y,Z*). As discussed above, Taurus A and B are overlayed in the (*X,Z*) projection, and the relative motions can be misleading. In the (*X,Y*) projection, Taurus A and B are converging to a common point, while in the (*Y,Z*) projection, Taurus B is moving in the direction of Taurus A. This might be evidence that the two populations are merging. In two out of three projections, Taurus E appears to be approaching Taurus A and B.

Additional high-precision radial velocities of each member, in combination with astrometric data, are required to understand the dynamics of the entire region.

[3] We used the implementation of the gal_uvw.pro IDL routine available in the public *astrolib* library, presented by Gagné et al. (2014).
[4] For the solar motion we adopt the value of (U,V,W)⊙ = (−8.5, 13.38, 6.49) from Coskunoğlu et al. (2011).

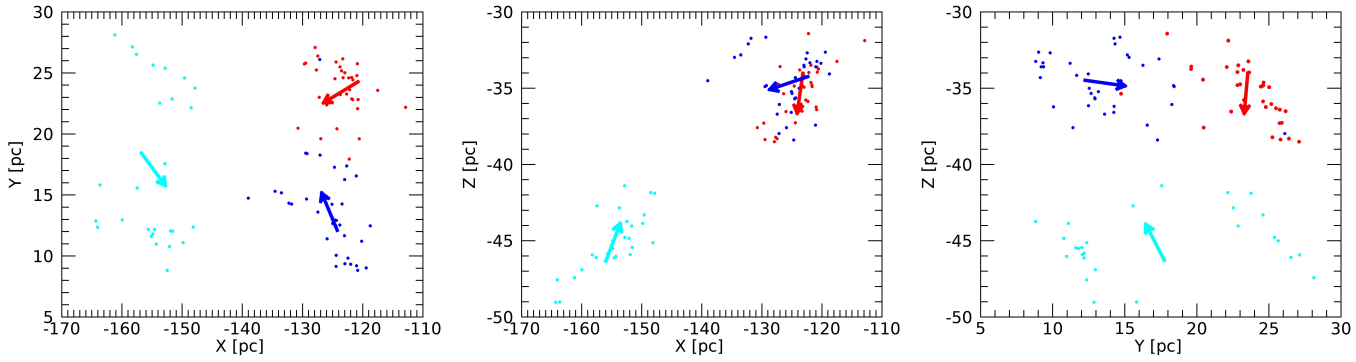

Fig. 8. Spatial distribution (as in Fig. 7) of Taurus A (red), B (blue), and E (cyan), represented by the small dots, with RV measurements. The arrows represent the differential space velocities (U,V,W) with respect to the mean motion between all the sources of the three populations. Each differential value has been magnified by 100.

5. Summary and conclusions

We carried out a statistical analysis (taking into account errors and covariances between the parameters) of the Taurus members with a reliable *Gaia* DR2 counterpart in order to look for multiple populations in the Taurus complex. Our results allow us to infer detailed information on the relation between the stellar population and the molecular cloud structures in the *Herschel* maps. We find six stellar populations. Three of them are located over *Taurus Main*: Taurus A and B at a similar distance of ∼130 pc, and Taurus E at ∼160 pc. We find that these stellar populations lie at a similar distance to the molecular cloud when this is structured as a cloud, suggesting that they are associated. This is not the case when the molecular cloud is filamentary. Taurus C and F are mostly concentrated on the L1517 and L1551 clouds. The sixth population, Taurus D, is widely spread spatially and kinematically, suggesting it could either be a sparse young population, or be composed of multiple substructures.

The analysis of the differential average velocity suggests that Taurus A and B might be merging, while Taurus E is proceeding towards Taurus A and B. However, a definitive conclusion on their kinematics will only be possible when accurate radial velocities become available for all the members.

This study supports the view that star formation occurred in clumpy and filamentary structures that are evolving independently, and that Taurus is not the result of the expansion of a single star-formation episode.

Acknowledgements. We thank the referee for his/her comments who helped to significantly improve the paper. This project has received funding from the European Union's Horizon 2020 research and innovation programme under the Marie Sklodowska-Curie grant agreement No 664931. This work has made use of data from the European Space Agency (ESA) mission *Gaia* (https://www.cosmos.esa.int/gaia), processed by the *Gaia* Data Processing and Analysis Consortium (DPAC, https://www.cosmos.esa.int/web/gaia/dpac/consortium). Funding for the DPAC has been provided by national institutions, in particular the institutions participating in the *Gaia* Multilateral Agreement. V.R. acknowledges the inspiring discussions with Steve.

References

André, P., Men'shchikov, A., Bontemps, S., et al. 2010, A&A, 518, L102
Armstrong, J. J., Wright, N. J., & Jeffries, R. D. 2018, MNRAS, 480, L121
Bailer-Jones, C. A. L. 2015, PASP, 127, 994
Cantat-Gaudin, T., Mapelli, M., Balaguer-Núñez, L., et al. 2019, A&A, 621, A115
Coskunoğlu, B., Ak, S., Bilir, S., et al. 2011, MNRAS, 412, 1237
Dale, J. E., Ercolano, B., & Bonnell, I. A. 2012, MNRAS, 424, 377
Dzib, S. A., Loinard, L., Ortiz-León, G. N., Rodríguez, L. F., & Galli, P. A. B. 2018, ApJ, 867, 151
Esplin, T. L., & Luhman, K. L. 2019, AJ, 158, 54
Franciosini, E., Sacco, G. G., Jeffries, R. D., et al. 2018, A&A, 616, L12
Gaczkowski, B., Preibisch, T., Stanke, T., et al. 2015, A&A, 584, A36
Gaczkowski, B., Roccatagliata, V., Flaischlen, S., et al. 2017, A&A, 608, A102
Gagné, J., & Faherty, J. K. 2018, ApJ, 862, 138
Gagné, J., Lafrenière, D., Doyon, R., Malo, L., & Artigau, É. 2014, ApJ, 783, 121
Gagné, J., Faherty, J. K., & Mamajek, E. E. 2018, ApJ, 865, 136
Galli, P. A. B., Loinard, L., Ortiz-Léon, G. N., et al. 2018, ApJ, 859, 33
Galli, P. A. B., Loinard, L., Bouy, H., et al. 2019, A&A, 630, A137
Goldsmith, P. F., Heyer, M., Narayanan, G., et al. 2008, ApJ, 680, 428
Goodman, A. A., Jones, T. J., Lada, E. A., & Myers, P. C. 1992, ApJ, 399, 108
Großschedl, J. E., Alves, J., Meingast, S., et al. 2018, A&A, 619, A106
Hacar, A., Alves, J., Burkert, A., & Goldsmith, P. 2016, A&A, 591, A104
Hacar, A., Tafalla, M., Kauffmann, J., & Kovács, A. 2013, A&A, 554, A55
Hartmann, L. 2002, ApJ, 578, 914
Jeffries, R. D., Jackson, R. J., Cottaar, M., et al. 2014, A&A, 563, A94
Kenyon, S. J., Dobrzycka, D., & Hartmann, L. 1994, ApJ, 108, 1872
Kirk, J. M., Ward-Thompson, D., Palmeirim, P., et al. 2013, MNRAS, 432, 1424
Krause, M. G. H., Burkert, A., Diehl, R., et al. 2018, A&A, 619, A120
Lindegren, L. 2018, Re-normalising the astrometric chi-square in Gaia DR2, gAIA-C3-TN-LU-LL-124
Lindegren, L., Madsen, S., & Dravins, D. 2000, A&A, 356, 1119
Luhman, K. L. 2018, AJ, 156, 271
Luri, X., Brown, A. G. A., Sarro, L. M., et al. 2018, A&A, 616, A9
Myers, P. C. 2009, ApJ, 700, 1609
Palla, F., & Stahler, S. W. 2002, ApJ, 581, 1194
Palmeirim, P., André, P., Kirk, J., et al. 2013, A&A, 550, A38
Preibisch, T., & Smith, M. D. 1997, A&A, 322, 825
Roccatagliata, V., Dale, J. E., Ratzka, T., et al. 2015, A&A, 584, A119
Roccatagliata, V., Sacco, G. G., Franciosini, E., & Rand ich, S. 2018, A&A, 617, L4
Schlafly, E. F., Green, G., Finkbeiner, D. P., et al. 2014, ApJ, 786, 29
Schmalzl, M., Kainulainen, J., Quanz, S. P., et al. 2010, ApJ, 725, 1327
Sicilia-Aguilar, A., Henning, T., Kainulainen, J., & Roccatagliata, V. 2011, ApJ, 736, 137
Sicilia-Aguilar, A., Henning, T., Linz, H., et al. 2013, A&A, 551, A34
Torres, R. M., Loinard, L., Mioduszewski, A. J., & Rodríguez, L. F. 2007, ApJ, 671, 1813
Torres, R. M., Loinard, L., Mioduszewski, A. J., & Rodríguez, L. F. 2009, ApJ, 698, 242
Torres, R. M., Loinard, L., Mioduszewski, A. J., et al. 2012, ApJ, 747, 18
Yan, Q.-Z., Zhang, B., Xu, Y., et al. 2019, A&A, 624, A6
Zari, E., Hashemi, H., Brown, A. G. A., Jardine, K., & de Zeeuw, P. T. 2018, A&A, 620, A172
Zucker, C., Speagle, J. S., Schlafly, E. F., et al. 2019, ApJ, 879, 125

Appendix A: Additional material

Here, Table A.1 provides a reduced version of the complete table of membership probabilities; the complete table is available at the CDS. Figure A.1 shows the 3D spatial distribution of the six populations, which can be rotated in the electronic version of the paper. The histograms in Fig. A.2 show the distribution of the radial velocity compiled from the literature for Taurus A, B, and E.

Table A.1. Reduced first ten lines of the table available at the CDS.

Name	*Gaia* DR2 ID	RA	Dec	PLX	E_PLX	PMRA	E_PMRA	PMDE	E_PMDE	
AB Aur	156917493449670656	73.9410446	30.5510888	6.13996	0.05709	3.92615	0.09673	−24.11163	0.06753	...
CX Tau	162758236656524416	63.6994652	26.8029627	7.81673	0.03963	9.02460	0.10009	−22.45099	0.06506	...
DL Tau	148010281032823552	68.4128640	25.3438374	6.27593	0.04767	9.32913	0.08686	−18.29044	0.06509	...
FM Tau	163184366130809472	63.5566418	28.2135524	7.57948	0.04656	8.58744	0.10322	−24.41631	0.06664	...
FT Tau	149623711269425408	65.9133224	24.9371978	7.82449	0.05194	6.91801	0.11914	−21.69847	0.07524	...
GM Tau	148449845165337600	69.5889388	26.1537301	7.22990	0.14906	5.46909	0.26974	−22.97363	0.21549	...
GO Tau	148106316500918272	70.7628400	25.3384431	6.91711	0.04803	4.72669	0.10092	−20.20513	0.04601	...
HD 28354	152189662169148288	67.3326699	27.4041113	7.28903	0.10899	7.26521	0.17405	−25.14882	0.13331	...
LkCa 15	144936836795636864	69.8241791	22.3508662	6.29465	0.04814	10.47118	0.12711	−17.38300	0.05969	...
LkCa 19	156900622818205312	73.9040623	30.2985351	6.26297	0.07864	4.30736	0.15384	−24.13216	0.07560	...

	ruwe	p_A	p_B	p_C	p_D	p_E	p_F	RV	SpType	Pop	Clust	Mem
...	1.02	0.00	0.00	0.98	0.02	0.00	0.00	8.90	A0	cyan	1	1
...	1.09	0.41	0.59	0.00	0.00	0.00	0.00	16.63	M2.5	red	7	0
...	1.16	0.00	0.00	0.00	0.01	0.99	0.00	13.94	K5.5	blue	13	1
...	1.27	1.00	0.00	0.00	0.00	0.00	0.00	...	M4.5	red	7	1
...	1.09	0.00	0.99	0.00	0.00	0.00	0.00	17.24	M3	red	9	1
...	1.23	0.01	0.91	0.00	0.08	0.00	0.00	16.46	M5	red	14	0
...	1.09	0.00	0.24	0.00	0.76	0.00	0.00	15.42	M2.3	red	15	1
...	1.10	0.99	0.00	0.00	0.01	0.00	0.00	...	B9	red	7	0
...	1.18	0.00	0.00	0.00	0.00	1.00	0.00	17.65	K5.5	blue	18	0
...	1.02	0.00	0.00	1.00	0.00	0.00	0.00	13.58	K2	cyan	1	1

Notes. RA and Dec positions and the astrometric data are from *Gaia*, the spectral types and the colors in the "pop" column are from Luhman (2018), the "clust" and "mem" columns are the cluster number and membership from Galli et al. (2019).

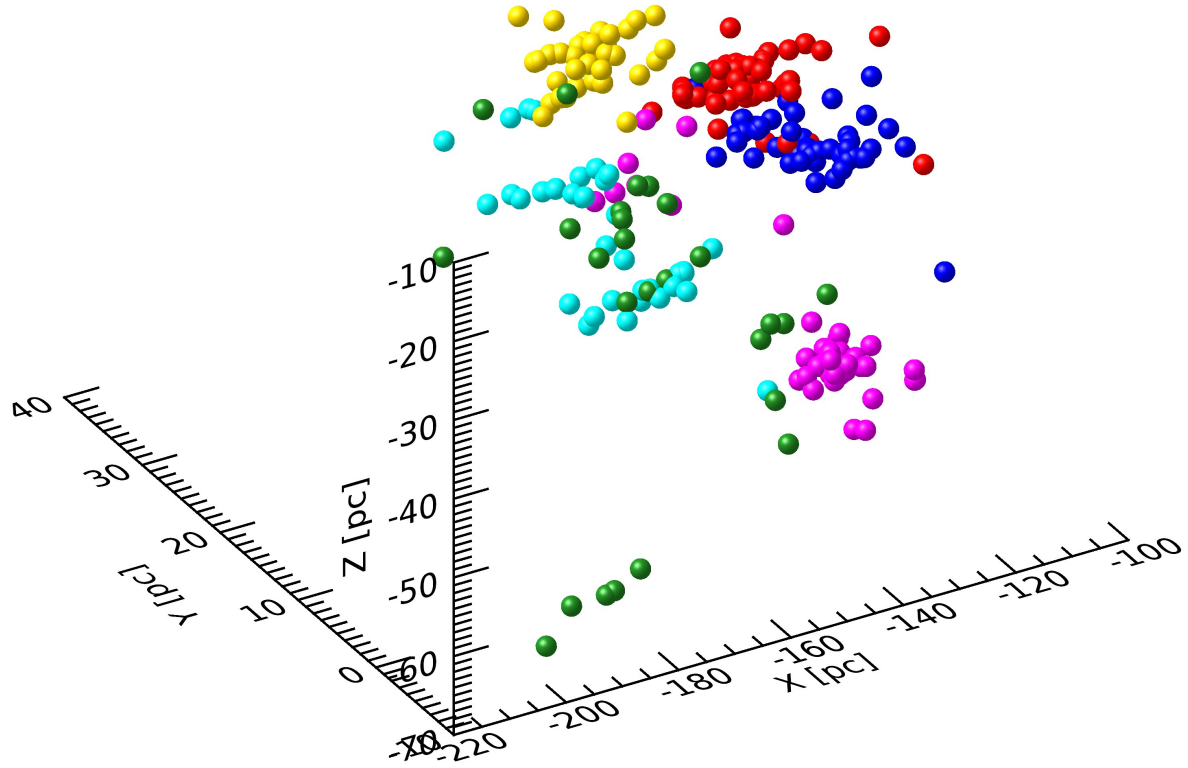

Fig. A.1. Three-dimensional spatial distribution of the multiple populations. The color code is as in Fig. 4. An animation with different orientation of this plot is available online.

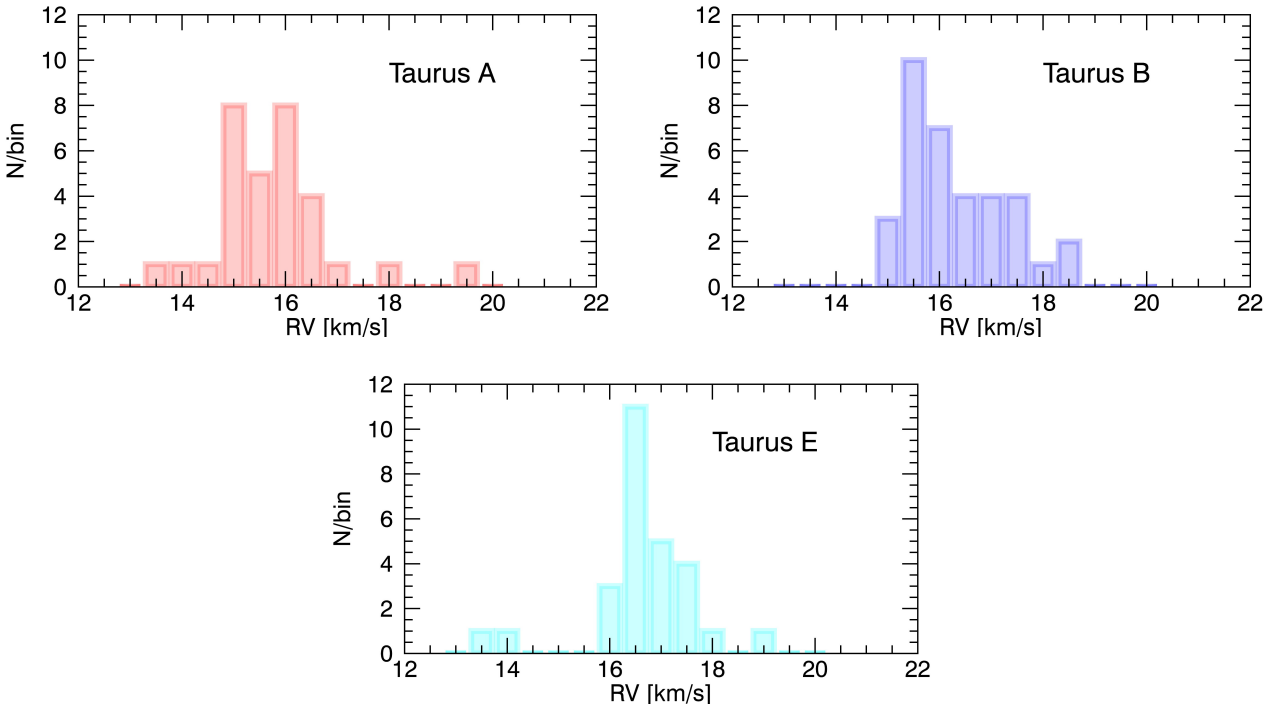

Fig. A.2. Distribution of radial velocities from Galli et al. (2019) for the most probable members of the Taurus A (red), Taurus B (blue), and the Taurus E (cyan) populations.